Research Square

Preprints are preliminary reports that have not undergone peer review.
They should not be considered conclusive, used to inform clinical practice,
or referenced by the media as validated information.

Single-cell transcriptomics reveals age-specific epithelial evolution and metabolic vulnerability in young breast cancer

JiangYang Wan
The Affiliated Huaian No.1 People's Hospital of Nanjing Medical University
Rui Peng Zhao
The Affiliated Huaian No.1 People's Hospital of Nanjing Medical University
Chen Zhang
The Affiliated Huaian No.1 People's Hospital of Nanjing Medical University
Wei Song
The Affiliated Huaian No.1 People's Hospital of Nanjing Medical University
LinLin Zhen
The Affiliated Huaian No.1 People's Hospital of Nanjing Medical University
DongZhu Da
The Affiliated Huaian No.1 People's Hospital of Nanjing Medical University
Zhi Li
drlz2018@njmu.edu.cn

The Affiliated Huaian No.1 People's Hospital of Nanjing Medical University

Research Article

Keywords: Breast cancer, Oxidative phosphorylation, Single-cell RNA sequencing, Tumor microenvironment, Age-specific therapy

Posted Date: August 21st, 2026

DOI: https://doi.org/10.21203/rs.3.rs-10323846/v1

License: This work is licensed under a Creative Commons Attribution 4.0 International License.
Read Full License

Additional Declarations: No competing interests reported.

Abstract

Young breast cancer (BC) patients under 40 years of age exhibit more aggressive disease and poorer clinical outcomes compared with older patients; however, the cellular and molecular basis underlying this age-associated disparity remains incompletely understood. In this study, we performed single-cell RNA sequencing (scRNA-seq) analysis of matched tumor and normal breast tissues from young and older BC patients, followed by unsupervised clustering and pseudotime trajectory analysis to dissect epithelial cell heterogeneity and developmental relationships. We identified two youth-specific hypermetabolic epithelial subpopulations characterized by significant upregulation of ATP synthesis and oxidative phosphorylation (OXPHOS)-related pathways, suggesting enhanced metabolic adaptability to stress conditions that may contribute to increased proliferative potential in young tumors. In addition, we discovered distinct epithelial subpopulations uniquely enriched in young normal breast tissue and demonstrated a clear developmental continuity between these normal epithelial states and tumor-specific subpopulations in young BC, indicating a potential age-dependent epithelial evolutionary trajectory. Functional validation further showed that pharmacological inhibition of OXPHOS using IACS-010759 selectively suppressed tumor growth and reduced intratumoral ATP levels in young tumor-bearing mice, supporting a metabolic vulnerability specific to young breast cancer. Collectively, our findings reveal distinct epithelial subpopulation architectures and immune microenvironmental differences between young and older BC patients, providing mechanistic insight into age-related tumor heterogeneity and highlighting OXPHOS-dependent metabolic reprogramming as a potential therapeutic target for young breast cancer.

Introduction

Breast cancer (BC) remains a leading global health burden, with young women often defined as diagnosed age < 40 years facing a disproportionately aggressive disease course characterized by larger tumors, higher metastatic potential, poorer treatment response and reduced survival compared to their older counterparts (1). While young age itself is established as an independent adverse prognostic factor, the underlying biological mechanisms driving this disparity are not fully elucidated (2, 3). Accumulating evidence suggests intrinsic molecular differences, including higher proliferative indices and distinct distributions of aggressive molecular subtypes in young patients, contribute significantly to their worse outcomes (4, 5). However, a comprehensive understanding of the cellular and transcriptional landscape distinguishing young and older BC, particularly regarding tumor metabolism, immune interactions and cellular heterogeneity, is still lacking.

Previous multi-omics studies have begun to decipher the molecular underpinnings of age-related disparity in BC. Genomically, younger patients exhibit a higher prevalence of germline mutations in high-penetrance genes such as BRCA1 and BRCA2. Transcriptomically, bulk RNA sequencing analyses have consistently identified that tumors from younger women are enriched for more aggressive intrinsic subtypes (e.g., basal-like, HER2-enriched) and display elevated proliferation signatures, as well as distinct gene expression programs related to metabolism and the DNA damage response (6).

Furthermore, investigations into the tumor immune microenvironment (TME) have revealed variations in immune cell composition, though findings have been inconsistent, potentially obscured by the limitations of bulk tissue analysis(7, 8). Critically, while these studies establish crucial associations, they offer a population-averaged view that fails to resolve the intratumoral heterogeneity. Consequently, they cannot determine whether the distinct transcriptional and metabolic signatures of young BC originate from a specific epithelial subpopulation, a shift in stromal or immune cell states, or altered cell-cell communication. The precise cellular origin, developmental trajectory, and functional drivers of aggressiveness in young BC thus remain incompletely understood.

A critical and confounding factor in dissecting age-specific biology is the distinct molecular subtype distribution between age groups. Notably, tumors in younger patients are enriched for more aggressive subtypes, particularly triple-negative breast cancer (TNBC), which is itself characterized by heightened metabolic activity and proliferation. This raises a key question: are the molecular and metabolic differences attributed to young age merely a reflection of this skewed subtype prevalence? Disentangling the effects of intrinsic subtype from those of host age requires analytical strategies that can either control for subtype or examine heterogeneity within subtype contexts.

Single-cell RNA sequencing (scRNA-seq) has revolutionized our ability to deconvolve tumor heterogeneity and identify rare cell subpopulations that drive pathogenesis (9). Unlike bulk transcriptomics, scRNA-seq enables precise mapping of cellular states and interactions within the tumor microenvironment at unprecedented resolution (10). Applying this technology to match tumor/normal tissues from 9 young (< 40 years) and 9 older (> 60 years) BC patients, we identified a dominant cancer cell subpopulation exclusively enriched in young tumors. This subpopulation exhibited pronounced upregulation of energy metabolism pathways, particularly ATP synthesis genes (e.g., ATP5F1B, ATP5MC3), revealing a metabolic vulnerability specific to young BC aggressiveness (11).

Aberrant energy metabolism is a recognized hallmark of cancer (12). Elevated ATP production provides critical bioenergetic support for energy intensive oncogenic processes, including MYC driven hyperproliferation and Rho GTPase dependent actin remodeling during invasion (13, 14). Furthermore, ATP acts as a central metabolic coordinator, directing carbon flux into nucleotide and lipid biosynthesis pathways to enable rapid biomass accumulation in dividing tumor cells (15, 16). Critically, heightened ATP reserves confer therapy resistance by activating drug efflux pumps and enhancing DNA damage repair capacity, thereby protecting tumors from chemo/radiotherapeutic assault (17, 18). Tumor cells frequently reprogram metabolic pathways to fuel rapid proliferation, invasion, and therapy resistance (19). Elevated ATP synthesis sustains energy intensive processes such as DNA repair and metastasis (17), traits aligning with the aggressive phenotype of young BC. Notably, recent studies correlate ATP overproduction with chemoresistance in TNBC (20) and immune evasion via extracellular adenosine accumulation (21), suggesting dual therapeutic implications. Our discovery of an ATP high subpopulation in young BC positions metabolic dysregulation as a central driver of their poor prognosis, potentially informing age specific therapeutic strategies.

Therefore, this study aims to: 1) Define the distinct single-cell transcriptional landscapes, including specific differential cell subpopulations, that characterize BC in young versus older women; 2) Investigate the role of heightened energy metabolism and ATP synthesis as a key driver of aggressiveness in young BC tumors and adjacent normal tissue; 3) Assess the preclinical efficacy of targeting energy metabolism pathways as a novel therapeutic strategy for young BC using murine models. By integrating deep molecular profiling with functional validation, we seek to provide a mechanistic explanation for the age disparity in BC prognosis and identify age-specific diagnostic markers and therapeutic targets.

Results

scRNA-seq analysis unveiled the heterogeneity in breast cancer between the young and the aged

Prior to correction, cells from different datasets exhibited significant technical clustering; however, Harmony effectively mitigated these inter-dataset technical variations while successfully preserving biological heterogeneity (Supplementary Fig. 1A). To investigate the difference of cellular heterogeneity between the young and aged, we initiated the processing and analysis of the sequencing data for 9 young breast cancer samples and 9 aged breast cancer samples. Following successful integration, we systematically evaluated two widely used non-linear dimensionality reduction algorithms, UMAP and t-SNE (Supplementary Fig. 1B, Fig. 1B). After conducting quality control and utilizing tSNE dimensionality reduction, we identify 8 distinct cell subsets comprising epithelial cells (n = 42,949) expressing EPCAM, T cells (n = 21,794) expressing CD3D, B cells (n = 4,922) expressing CD19 and CD79A, plasma cells (n = 3,417) expressing IGHG1 and MZB1, myeloid cells (n = 7,959) expressing CD68, endothelial cells (n = 7,660) expressing PECAM1 and VWF, fibroblasts (n = 23,520) expressing COL1A1 and COL1A2 and NK cells (n = 1,132) expressing GNLY and NKG7. The characteristic genes of each cell cluster are displayed using a Dot plot (Fig. 1A-1B). To further analyze the different composition of cell types between the young and aged, we conduct tSNE dimensionality reduction to map the cells of breast tumors (Fig. 1C). Compared to the aged group, the young group showed decreased proportions of epithelial cells and increased proportions of fibroblasts (Fig. 1D). We further quantified the relative proportions of these lineages to assess whether age-related differences existed at the global cellular level. Quantitative analysis revealed that the overall cellular composition was remarkably stable between the two groups. No statistically significant differences were observed in the proportions of Epithelial cells (P = 0.97), T cells (P = 0.48), B cells (P = 0.83), or Myeloid cells (P = 0.77). Similarly, the frequencies of stromal components, such as Fibroblasts (P = 0.44) and Endothelial cells (P = 0.59), remained comparable across age groups (Supplementary Fig. 1C).

In order to filter out normal epithelial cells, Copycat algorithm was further used to identify aneuploid epithelial cells and diploid epithelial cells. Finally, we defined aneuploid cells as tumor cells (n = 24,874) and diploid epithelial cells as normal cells (n = 15,928). With tSNE, we mapped the tumor epithelial cells

and normal epithelial cells in breast tumors (Fig. 1E). As the changes in the proportions of epithelial cells were significant, we believe that epithelial cells play a crucial role in the development of breast cancer. Next, we performed unsupervised clustering on normal epithelial cells and tumor epithelial cells respectively. As a result, we obtained 14 normal epithelial cell subclusters and 16 tumor epithelial cell subclusters. Based on the functions and marker genes of the 14 normal epithelial cell subclusters and 16 tumor epithelial cell subclusters, we further consolidated them into normal and tumor major epithelial cell subclusters respectively. This consolidation was guided by the shared characteristics and biological relevance of the original subclusters (Supplementary Fig. 1).

Finally, we observed further heterogeneity with 9 subclusters in normal epithelial cells (nC1 through nC9) and tumor epithelial cells (tC1 through tC9), each cluster containing unique marker gene profiles (Fig. 1F). In normal epithelial cells, nC1 and nC3 each accounted for approximately 25%, nC2 for about 13%, being the major subclusters. nC7 accounted for around 11%, while nC4, nC5, and nC6 had proportions of about 8%, 7%, and 6% respectively. nC8 and nC9 were the least abundant, each making up approximately 3% (Fig. 1G). In the tumor epithelial cells, tC4 was the most abundant, accounting for approximately 20%. tC1 and tC5 each made up about 14%, also being major subclusters. tC3 and tC7 accounted for around 12% each, while tC2 and tC8 each had a proportion of approximately 8%. tC6 accounted for about 7%, and tC9 was the least abundant at around 5% (Fig. 1H).

Definition and functional distinctions of epithelial cell subclusters revealed the difference between the young and aged group

To identify tumor subclusters that exert unique roles in the young population, we employed tSNE analysis to map the proportional differences among epithelial cell subclusters (Fig. 2A). Normal and tumor epithelial cells were analyzed through independent clustering to maintain state-specific resolution. Initially, we identified 15 normal and 17 tumor clusters. These were further consolidated into 9 normal (nC1–nC9) and 9 tumor (tC1–tC9) sub-clusters based on the similarity of their top 3 highly variable genes (HVGs) and overlapping functional signatures, as detailed in Supplementary Fig. 1. As the bar plot shown, tC3 (highly expressing CDKN2A) and tC9 (highly expressing NDUFC2) exhibited specific expression patterns exclusively in the young group, whereas tC5 (highly expressing KRT15), tC6 (highly expressing HIST3H2A) and tC1 (highly expressing TFF1) demonstrated pronounced overexpression uniquely within the aged group (Fig. 2B). These different expression profile highlights potential age-related heterogeneity in epithelial cells. Next, we analyzed the differences between each subcluster and the other cell subclusters. Then, we selected the DEGs for further GO enrichment analysis (Supplementary Fig. 2). GO enrichment analyses suggested that the main functions of tC3 were involved in the ATP metabolic process, oxidative phosphorylation and aerobic respiration (Fig. 2C). The main functions of tC9 were involved in Golgi vesicle transport and response to endoplasmic reticulum stress (Fig. 2D). tC5 cluster cells may possess a relatively primitive cellular state, exhibiting the capacity to differentiate into multiple cellular morphologies (Fig. 2E). The main functions of tC1 were involved in RNA splicing (Fig. 2F). The main functions of tC6 were involved in antigen processing and presentation of peptide antigen via MHC class I (Fig. 2G). To further characterize the functional identity and biological

differences among the identified tumor epithelial subclusters, we conducted GSEA based on the ranked gene lists of each subtype. Tumor Epithelial Type 3 was predominantly enriched in pathways associated with high metabolic activity, specifically Oxidative Phosphorylation and ATP Synthesis. In contrast, Tumor Epithelial Type 9 exhibited strong enrichment in Cellular Responses to Stimuli and ER-to-Golgi Anterograde Transport. Type 1 was enriched in MHC Class I Antigen Processing and Presentation, while Type 5 displayed activation of Receptor Tyrosine Kinase (RTK) signaling and general cancer pathways (Supplementary Fig. 3C).

To validate the effectiveness of marker genes in discriminating subclusters across different age groups, tSNE projection was utilized to map the major marker gene of tC3/tC9/tC5/tC6/tC1. tSNE visualization showed that CDKN2A, NDUFC2, KRT15, HIST3H2A and TFF1 exhibited specific and high expression within respective subclusters (Fig. 2C-2G). Furthermore, we performed histological staining on BC tissue from both the young group and aged group. The results showed that CDKN2A and NDUFC2 were specifically overexpressed in young breast tumor tissues and KRT15, HIST3H2A and TFF1 were specifically overexpressed in the aged breast tumor tissues (Fig. 2H-2L).

Analyses reveal distinct epithelial cells differentiation trajectories between the young and aged

After the clustering and functional analyses of tumor epithelial cells, we aimed to describe their developmental trajectories and cell fate transitions from normal epithelial cells through pseudotime analysis. First, we employed tSNE analysis to map the proportional differences among normal epithelial cell subclusters (Fig. 3A). As the bar plot shown, nC2(highly expressing CDKN2A), nC5 (highly expressing CD24) and nC9 (highly expressing KRT17) exhibited specific expression patterns exclusively in the young group, whereas nC4 (highly expressing ZNF90), nC6 (highly expressing KRT15) and nC8 (highly expressing CRISP3) demonstrated pronounced overexpression uniquely within the aged group (Fig. 3B). Subsequently, we constructed the developmental trajectories of all normal epithelial cell subclusters and crucial tumor epithelial cell subclusters tC3/tC9/tC5/tC6/tC1 respectively.

The pseudotime trajectory analysis of all normal epithelial subclusters and tumor epithelial cells type 3(tC3) was conducted to evaluate the responses of the normal epithelial subclusters to tC3 specifically expressed in young tumor tissues (Fig. 3C). The development to tumor epithelial cells type 3 could be divided into nine differentiation states and nC2 specifically expressed in young tumor tissues shared state1 with tC3(Fig. 3D-3E). GO enrichment analyses suggested that the main functions of nC2 were involved in the ATP metabolic process, oxidative phosphorylation and aerobic respiration, which are same with the main functions of tC3(Fig. 3F). The pseudotime trajectory analysis of all normal epithelial subclusters and tC9 specifically expressed in young tumor tissues showed that nC3, nC7 and nC8 and tC9 shared the state1(Fig. 3G-3I). GO enrichment analyses suggested that the main functions of nC3 were involved in aerobic respiration and oxidative phosphorylation. The main functions of nC7 were

involved in antigen processing and presentation of peptide antigen (Fig. 3J). The main functions of nC8 were involved in aerobic respiration and oxidative phosphorylation (Fig. 4D).

The pseudotime trajectory analysis of all normal epithelial subclusters and tumor epithelial cells type 5(tC5) was conducted to evaluate the responses of the normal epithelial subclusters to tC5 specifically expressed in the aged tumor tissues (Fig. 4A). The development to tumor epithelial cells type 5 could be divided into nine differentiation states and nC6 specifically expressed in young tumor tissues shared state 7 with tC5 (Fig. 4B-4C). GO enrichment analyses suggested that the main functions of nC6 were involved in limb morphogenesis and appendage morphogenesis (Fig. 4H). The pseudotime trajectory analysis of all normal epithelial subclusters and tC6 specifically expressed in the aged tumor tissues showed that nC4 specifically expressed in the aged tumor tissues and tC9 shared the state 9(Fig. 4E-4G). GO enrichment analyses suggested that the main functions of nC4 were involved in RNA splicing (Fig. 4L). The pseudotime trajectory analysis of all normal epithelial subclusters and tC1 specifically expressed in the aged tumor tissues showed that nC3, nC8 and tC9 shared the state 3(Fig. 4I-4K). Hence, we supposed that high-metabolic, ATP-synthesis-driven epithelial cells type contributes to young BC aggressiveness.

The pseudotime analysis revealed distinct developmental trajectories for various cell lineages. Starting from nC2 to tC3, the trajectory split into five branches, with no significant changes in nC2 and tC3 marker genes (Fig. 5A-5B). A heatmap of major branch 1 showed differential gene expression profiles (Fig. 5C), with DDIT4 playing a crucial role in ATP metabolism and oxidative phosphorylation, suggesting its involvement in the aggressiveness of young BC cells. From nC3, nC7, and nC8 to tC9, the trajectory diverged into one branch (Fig. 5D). Markers CHCHD1, NDUFC2, and SPCS2 showed significant upregulation in tC9 (Fig. 5E), with a heatmap displaying gene expression profiles at major branch 1 (Fig. 5F). For the nC6 to tC5 trajectory, it split into four branches with stable marker gene expression (Fig. 6A-6B). A heatmap detailed gene expression at major branch 1 (Fig. 6C). The nC4 to tC6 trajectory diverged into one branch with no significant marker gene changes (Fig. 6D-6E). A heatmap showed gene expression profiles at major branch 1 (Fig. 6F). Lastly, the nC3 and nC8 to tC1 trajectory split into three branches, with AGR1, NDUFC2 and SPCS2 significantly increasing in tC1(Fig. 6G-6H). A heatmap illustrating gene expression at major branch 1 (Fig. 6I).

Immune microenvironment of BC exhibits significant heterogeneity between the young and aged

The cell-cell communication network among different cell types in breast cancer was shown in Fig. 7. Compared to the normal epithelial cells, tumor epithelial mainly interacted with cell types including B cells and T cells (Fig. 7), indicating immune microenvironment may played a crucial role in the development of breast cancer. The cell-cell communication network among other cell types in breast cancer was shown in Supplementary Fig. 2. Tumor epithelial cells functioned as major senders in the WNT, TRAIL, and VEGF pathways. Notably, the TRAIL and WNT signaling networks showed robust

autocrine interactions within the tumor compartment and paracrine signaling toward T cells. Fibroblasts emerged as a primary signaling hub, exhibiting dominant outgoing signaling in the TGFb, IGF, and MK pathways, which are known to modulate extracellular matrix remodeling and tumor growth (Supplementary Fig. 4C).

To further investigate heterogeneity of immune microenvironment between the young and aged, the difference proportional composition of B cells, T cells and myeloid cells between the young and the aged was illustrated (Fig. 7C-E). With tSNE, we mapped the B cells landscape of breast tissues in the young and aged group and identified 6 major cell types, including memory B cells (highly expressing CD19, MS4A1 and CD27), folicular B Cells (highly expressing CXCR5), regulatory B Cells (highly expressing CD19 and CD24), activated B Cells (highly expressing CD19, CD86 and HLA-DR), DN B Cells (negatively expressing CD27 and IgD) and Marginal Zone-like B Cells (highly expressing CD19 and CD21) (Fig. 7C). Memory B cells constitute approximately 44% of the total B cell population, which is notably lower compared to the old group where they make up around 57%. Regulatory B cells are more prevalent in the young group, accounting for about 29%, whereas they represent approximately 14% in the old group. These findings suggest that the young group has a distinct B cell composition characterized by higher proportions of regulatory B cells, and lower proportions of activated and memory B cells compared to the old group. To further resolve the cellular landscape of the immune microenvironment, we performed fine-grained sub-clustering of B-cells, T-cells, and myeloid cells. The identity of each sub-population was confirmed by the expression of canonical lineage and functional markers as visualized in Supplementary Fig. 5C.

The analysis of T cell subsets in both aged and young groups reveal distinct differences in their distribution and composition (Fig. 7D). In the aged group, Th2 cells (highly expressing CD4 and FOXP3) represent approximately 16% of the total T cell population, while in the young group, this proportion drops to about 2%. Th1 cells (highly expressing CXCR3 and IFNG) are more prevalent in the aged group at around 18% compared to the young group, where they constitute only about 16%. CD8 + CTL cells (highly expressing CD8A and CD3E) are significantly more prevalent in the young group at around 45% compared to the aged group, where they make up about 37%. These findings suggest that the distribution of T cell subsets varies significantly between the aged and young groups, with the aged group having higher proportions of Th1 and Th2 cells, while the young group has higher proportions of CD8 + CTL cells and Trm cells (highly expressing CD69 and ITGAE) and Treg cells (highly expressing CD4 and IL2RA).

The results depicted in the t-SNE plots (Fig. 7E) and the bar chart illustrate significant differences in the distribution and composition of myeloid cells between aged and young samples. SPP1 + TAMs (Tumor-Associated Macrophages) (highly expressing CD68 and SPP1) are more prevalent in the young group, accounting for approximately 39%, compared to the aged group where they make up about 25%. M1 TAMs (highly expressing CD86 and FCGR1A) are less abundant in the aged group at around 12% compared to the young group, where they constitute about 19%. CXCL9 + TAMs (highly expressing CD68 and CXCL9) are slightly more prevalent in the aged group at about 2% compared to the young group,

where they account for approximately 6%. cDCs (conventional Dendritic Cells) (highly expressing THBD and CD1C) are more abundant in the aged group, making up approximately 28%, compared to the young group, where they constitute around 16%. M2 TAMs (highly expressing CD163 and FCER2) are less abundant in the aged group at about 3% compared to the young group, where they account for approximately 9%. RTM-TAMs (highly expressing LYVE1 and HES1) are slightly more prevalent in the aged group at around 11% compared to the young group, where they make up about 3%. TREM2 + TAMs (highly expressing CD68 and TREM2) are more abundant in the aged group, accounting for approximately 18%, compared to the young group where they make up about 8%.

These findings suggest that the distribution of immune cell subsets varies significantly between the aged and young groups.

IACS-010759 effectively inhibited young breast cancer progression in mice

We utilized a cohort of 15 young and 15 aged BALB/c mice for this study. All mice received in situ injections of 4T1 cells to establish tumors. The growth environment for the cells was determined by the mice's age status, simulating the pathological conditions of tumors in young and aged.. Subsequently, mice within each age group were divided into subgroups (n = 5) and administered either the oxidative phosphorylation inhibitor IACS-010759 or doxorubicin and an equivalent volume of PBS (Fig. 8A). Tumor growth was monitored longitudinally (Fig. 8C), and final tumor morphology was documented photographically (Fig. 8B). The results showed that in the control (PBS) groups, tumors in young mice were moderately larger than those in aged mice, although this difference did not reach statistical significance (p = 0.1851, CI= [-0.1376, 0.6038]). However, following administration of IACS-010759, a significant suppression of tumor growth was observed specifically in young mice (p = 0.0015, CI= [-0.9927, -0.3409]). In contrast, the inhibitory effect of IACS-010759 on tumor volume in aged mice was markedly less pronounced compared to its efficacy in the young cohort (p = 0.2388, CI= [-0.1729, 0.5992]). Whereas, the tumor-suppressing effect of IACS-010759 remains inferior to that of doxorubicine (p = 0.0087, CI= [-0.9067 to -0.1797]). Fortunately, all mice treated with IACS-010759 maintained stable weight gain, whereas weight gain was significantly suppressed in the doxorubicin-treated group. This indicates that at the administered dose, IACS-010759 exhibited no apparent systemic toxicity (Fig. 8D). Then, ATP concentrations and OXPHOS-related proteins ATP1A1, ATP5F1B, ATP5J2 and phosphorylated AMPK were measured in tumor tissues harvested at equivalent weights. It confirmed that IACS-010759 treatment effectively reduced ATP synthesis capacity and OXPHOS-related proteins expression within the tumor tissue of both young and aged mice compared to their respective PBS controls, although the reduction was not as significant as in the doxorubicin-treated group (Fig. 8E-F). To characterize the preclinical pharmacokinetics of IACS-010759, a series of blood samples were collected at designated time points following administration. Figure 8G showed the pharmacokinetic curve of IACS-010759 plasma concentration over time, along with the corresponding calculated parameters (Fig. 8H). Results indicated that after administration of IACS-010759, the concentration of luteolin in mouse plasma

exhibited a rapid rise followed by a gradual decline. Compared to the aged group, IACS-010759 demonstrated faster metabolism in young mice, manifested by earlier peak plasma concentrations, lower AUC values, and shorter half-lives. Taken together, we conclude that the use of inhibitors targeting ATP synthesis and oxidative phosphorylation is more effective in the treatment of young breast cancers.

Discussion

Our understanding of the distinct biological drivers underpinning the aggressive phenotype of young BC remains incomplete. As an exploratory analysis leveraging publicly available scRNA-seq datasets, this study provides an in-depth comparison of the transcriptional landscape and cellular heterogeneity distinguishing BC in young (< 40 years) and older (> 60 years) women, with a specific focus on metabolic dysregulation and immune contexture. While our integrated cohort contains matched tumor-normal samples, we acknowledge that it is not exclusively composed of such pairs; thus, our work is positioned as a hypothesis-generating study that uncovers robust, age-associated biological patterns at single-cell resolution. Within this framework, a key finding is the identification of a dominant, highly prevalent cellular subpopulation unique to young BC tumors, characterized by a profound upregulation of genes governing energy metabolism, particularly ATP synthesis pathways. Altered high-energy metabolism and ATP production patterns represent one of the core drivers of breast cancer progression. This metabolic reprogramming confers cancer cells with: proliferative advantage, environmental adaptability, resistance to cell death, and immune evasion capabilities. (11, 12, 26). Crucially, this metabolic signature was not exclusive to tumor cells, even within adjacent normal breast tissue from young women, we observed a baseline elevation in energy metabolism related gene expression compared to older women. This suggests a potential intrinsic, age dependent metabolic predisposition in the breast tissue milieu of younger individuals, which is associated with and may contribute to a microenvironment permissive for the development of aggressive, metabolically demanding tumors (27).

Notably, our scRNA-seq analysis revealed a distinct subpopulation in older BC characterized by specific overexpression of genes involved in cellular dedifferentiation programs and, based on GO enrichment, RNA splicing-related processes. This transcriptional signature is consistent with a state of heightened cellular plasticity and impaired differentiation, which may drive tumor heterogeneity. The elevated expression of spliceosome components suggests a potential alteration in the splicing machinery; however, we note that this study did not directly quantify alternative splicing events, and thus a direct link between this signature and functional splicing dysregulation, genomic instability, or therapy resistance remains to be established. Future studies incorporating long-read or full-length single-cell RNA sequencing to directly profile splice variants are warranted to validate this hypothesis and its clinical implications (28, 29).

Moreover, immunologic infiltration against young and older breast cancers showed interesting differences. While we observed evidence of active immune cell recruitment signals in young BC such as the activation of CD8 + CTLs and Trm cells and inhibition of Th1 cells, the overwhelming dominance of the high-metabolic subpopulation and a relative scarcity of specific stromal subpopulations crucial for

effective immune synapse formation and antigen presentation suggest a potential imbalance that could favor an immunosuppressive niche. This cellular composition is consistent with features often associated with a functionally "cold" tumor state (30, 31). However, definitive classification would require additional functional metrics such as T-cell receptor (TCR) clonality, immune checkpoint expression, and cytolytic activity scores, which were not assessed in this study.Conversely, compared to breast cancers in young hosts, the immune response in aged hosts appears attenuated, primarily characterized by increased immuno-suppressive Th1 cells proportion and reduced anti-tumor CD8 + CTLs proportion. This is frequently attributable to age-dependent impairments in adaptive immunity and advancing immunosenescence (32). However, older BC showed a distinct cellular subset exhibiting elevated expression of MHC class I molecules, which are critical for antigen presentation (33). This feature could enhance tumor immunogenicity and facilitate immune recognition, suggesting a more permissive microenvironment for immune-stromal crosstal (34). Whether this translates to a clinically meaningful difference in responsiveness to immunotherapy remains speculative and requires prospective clinical validation.

The functional significance of this heightened energy metabolism in young BC was further explored in vivo. Utilizing young and aged syngeneic mouse mammary tumor models, we demonstrated a significantly enhanced therapeutic response to pharmacological agents targeting key energy metabolism pathways specifically the OXPHOS inhibitor IACS-010759 (19, 35). Strikingly, IACS-010759, a potent and selective inhibitor of mitochondrial complex I (36), achieved superior tumor regression in young host tumors compared to aged hosts, corroborating the heightened metabolic dependency of young BC on OXPHOS for ATP production. This age specific efficacy aligns with the mechanism of IACS-010759: it cripples tumors reliant on mitochondrial respiration (37), precisely the vulnerability identified in our scRNA-seq data. Notably, the drug's limited efficacy in aged models may reflect their lower baseline OXPHOS activity and/or compensatory glycolytic flux, underscoring the necessity of age stratified metabolic targeting. This differential sensitivity highlights a strong association between OXPHOS dependency and young host age, and supports further investigation into targeting metabolic pathways as a potential age-specific strategy (38). However, given that the mouse experiments are underpowered (n = 5 per group), we need to conduct more extensive studies in large animals regarding drug efficacy, metabolism, distribution, and adverse effects before it can be reasonably advanced to clinical trials. Moreover, our study preliminarily reveals a correlative link between a high-metabolic epithelial state and young BC. Multicenter, large-sample validation studies are crucial for implementing preliminary conclusions. Also, to establish direct causality, that this metabolic program drives aggressiveness, future work employing genetic or pharmacological perturbation of key regulators identified in our study is essential. Functional assays, such as CRISPR-based gene knockdown in young patient-derived organoids or xenografts, coupled with measurements of proliferation, invasion, and therapy resistance, will be needed to definitively validate this metabolic subpopulation as a functional driver of poor prognosis.

Materials and Methods

Datasets acquisition

For our study, we utilized single-cell RNA sequencing (scRNA-seq) data obtained from the Gene Expression Omnibus (GEO) database, specifically from the datasets EGAD00001006608, GSE161529, GSE176078, and GSE243526. Our analysis encompassed a comprehensive cohort of 18 breast tumor samples, evenly divided between patients under 40 years old as the young group and those over 60 years old as the aged group, ensuring a balanced representation of both age groups. For the integration of clinical metadata, we collected comprehensive pathological information for each sample, including age, molecular subtype, and TNM stage, as detailed in Table S1.

scRNA-Seq quality control and integration

The single-cell RNA sequencing (scRNA-seq) data analysis was conducted using the Seurat package (version 4.3.0). To ensure data quality, cells were filtered based on mitochondrial gene expression levels, excluding those exceeding 15% (22), and gene counts were restricted to a range between 300 and 5000 (23). The filtered cells then underwent a series of analytical steps including data normalization, identification of highly variable genes, scaling, and principal component analysis (PCA) to facilitate downstream analysis. To address potential batch effects in our merged scRNA-seq dataset, we employed the Harmony package, adhering to its recommended protocol. This harmonization process helped to minimize technical variations and improve the comparability of the data across different batches. Post harmonization, we applied the t-distributed Stochastic Neighbor Embedding (t-SNE) method for dimensionality reduction and visualization of the complex scRNA-seq data. This approach effectively captured the local structure of the data, allowing for the identification of distinct cell clusters. The FindNeighbors and FindClusters functions (with a resolution parameter set to 0.3) were used to delineate these clusters. Throughout the analysis, default parameters were maintained for all standard procedures to ensure consistency and reproducibility of the results. Detailed information regarding the scRNA-seq platform (10x Genomics Chromium), sequencing parameters, and the exact number of cells analyzed per sample (pre- and post-quality control) is now provided in Table S2.

Cell Annotation

To ensure accurate cell typing, we utilized the FindAllMarkers function to identify differentially expressed genes (DEGs) across various cell clusters. The identity of the eight major cell lineages was determined by the expression of classic marker genes. Specifically, Epithelial cells were identified by EPCAM and KRT19; T cells were defined by CD3D, CD3E, and CD8A; Myeloid cells were characterized by CD68, CD163, and CSF1R; B cells were marked by CD19 and MS4A1; Plasma cells by IGHG1 and MZB1; NK cells by NCR1 and GNLY; Fibroblasts by COL1A1 and DCN; and Endothelial cells by PECAM1 and VWF. The specificity of these markers is visualized in the dotplot in Fig. 1A. B cell Sub-populations were identified by pan-B markers CD19 and MS4A1. Subsets were further defined as Memory B cells (CD27, CXCR5), Activated B cells (CD86, HLA-DRA), and Follicular B cells (IGHD). T cell Sub-populations were

defined by the pan-T marker CD3E. CD8 + CTLs were identified by CD8A and effector molecules (GZMB, IFNG), while Exhausted T cells (Tex) were characterized by high expression of inhibitory receptors including PDCD1, LAG3, and HAVCR2. Regulatory T cells (Tregs) were specifically identified by the co-expression of FOXP3 and IL2RA. Myeloid-cell Subculsters were characterized by CD68 and CD14. Tumor-associated macrophages (TAMs) were further stratified into M1-like (CXCL9, CD86), M2-like (CD163, MRC1), and specialized SPP1 + or TREM2 + subsets. Dendritic cells (cDCs) were identified by CD1C and CLEC9A.

To differentiate between tumor cells and normal somatic cells within the epithelial population, we employed copy number variation (CNV) analysis using the CopyKAT version 1.6.10 algorithm. This method, which stands for Copy number Karyotyping of Aneuploid Tumors, enables the distinction between aneuploid tumor cells and diploid normal cells based on their CNV profiles. Additionally, we performed subclustering of T cells, B cells, and myeloid cells based on their specific known markers. This approach allowed us to further refine our cell classification and gain a more nuanced understanding of the cellular heterogeneity within the samples.

Pseudotime analysis

For the analysis of developmental trajectories, we employed the DDRTree algorithm within the Monocle2 framework, as previously described (24). Within this framework, we designated "ordering genes" as those that demonstrated significant high variability in expression, excluding any genes associated with cell cycle dynamics that had been previously identified. Utilizing the "reduceDimension" function, we constructed a DDRTree to facilitate the dimensionality reduction of our data. To define the cellular trajectory, we selected the top 4,000 highly variable genes (HVGs) identified by Seurat’s method. These 4,000 genes were chosen to maximize the capture of subtle transcriptomic variations across epithelial subsets, thereby increasing the resolution of the pseudotime trajectory and the accuracy of bifurcation point detection. After filtering for genes expressed in at least 10 cells, the final gene set was used for manifold learning via the DDRTree algorithm. Subsequently, the "orderCells" function was applied to arrange the cells along the developmental trajectory. This process allowed us to subdivide both young and aged epithelial cells into distinct subclusters for a more detailed pseudotime analysis. Based on the outcomes from Monocle2, epithelial cells along the main differentiation pathway were categorized into multiple states, providing a comprehensive view of their developmental progression.

Functional Enrichment Analysis

The Gene Ontology (GO) analysis was conducted to classify and enrich the functional annotations of the marker genes specific to epithelial cell subclusters. Initially, a comprehensive examination of all marker genes was performed against each category within the Gene Ontology database, accessible at Gene Ontology Resource. For each GO term, the corresponding gene count was determined. To pinpoint the GO terms that were significantly overrepresented among the differentially expressed genes (DEGs), a hypergeometric test was employed. The resulting p-values underwent Bonferroni correction to adjust for multiple testing, with a threshold of a corrected p-value ≤ 0.05 used to denote statistical significance. GO

terms that met this criterion were considered to be significantly enriched among the DEGs when analyzed against the comprehensive transcriptome background. This analytical approach effectively revealed the predominant biological functions linked to the epithelial cell subclusters under investigation.

Gene Set Enrichment Analysis (GSEA) using the R package clusterProfiler was used to investigate the functional biological programs and signaling pathways activated in specific tumor cell subpopulations. All detected genes were ranked in descending order based on their log2 fold change (log2FC) derived from the differential expression analysis, ensuring that highly up-regulated genes were positioned at the top of the ranked list. This ranked list was then queried against the Canonical Pathways (C2: CP) sub-collection from the Molecular Signatures Database (MSigDB, v2023.2), which encompasses curated pathways from KEGG, Reactome, and Biocarta. The enrichment score (ES) was calculated using a weighted Kolmogorov-Smirnov statistic, and statistical significance was estimated through 1,000 permutations.

Cell-cell communication analysis

In order to explore the interactions between cells, we constructed separate computational objects for both young and aged groups using Seurat objects, following the CellChat (version 2.2.1) workflow. We accessed the CellChatDB.human dataset from the CellChatDB repository, focusing on four types of cell communication mechanisms: "Secreted Signaling," "ECM-Receptor," "No-protein Signaling," and "Cell-Cell Contact." Our analysis involved identifying ligands and receptors that were highly expressed and evaluating their interactions. To determine the likelihood of communication between different cell subpopulations, we employed the "computeCommunProb" function with the "truncatedMean" method. This approach facilitated the construction of a cell communication network. Following this, we conducted a comparative analysis of the CellChat objects for the young and aged groups. By examining the interaction strength between cells in a two-dimensional space, we were able to identify significant alterations in the signaling or reception of signals across the different age groups. This methodological strategy provided valuable insights into the cell-cell interactions within the context of age-related differences.

Immunohistochemical staining

The breast cancer tissue samples were initially fixed using a 4% paraformaldehyde (PFA) solution. Following fixation, the tissues underwent a dehydration process before being embedded in paraffin. Subsequently, sections of the paraffin-embedded tissues were carefully cut to a thickness ranging from 7 to 12 micrometers. For frozen tissue samples, sections were prepared at a uniform thickness of 12 micrometers. Immunohistochemical staining was applied to both the frozen and paraffin-embedded tissue sections. When required, a heat-induced antigen retrieval step was incorporated to enhance antibody binding. To reduce non-specific staining, the tissue sections were pre-incubated in a blocking solution containing 3% donkey serum. The primary antibodies employed in this study included rabbit

anti-CDKN2A (1:200), rabbit anti-NDUFC2 (1:500), rabbit anti-KRT15 (1:250), rabbit anti-HIST3H2A (1:250) and rabbit anti-TFF1 (1:250).

Breast cancer model in mice

Aged BALB/c mice (12–14 months, female) and young BALB/c mice (6–8 weeks, female) were purchased from (Gempharmatech, China). 5×10^5 4T1 cells with 100 μl phosphate buffered saline (PBS) were injected subcutaneously to the subcutaneous in mice. When the tumors volume was about 0.05–0.06 cm^3, all mice were divided into 3 groups and treated with PBS, IACS-010759 (Macklin, China) and doxorubicin (MedChemExpress,USA) respectively. IACS-010759 were taken orally at 5 mg/kg every two days and doxorubicin were taken by tail vein injection every 4 days. The growth of mice weights and tumors volume were recorded. After 2 weeks, the tumors were removed and photographed. The work has been reported in accordance with the ARRIVE guidelines (25).

ATP Measurement Assay

We weighed an equal mass of tumor tissue (20mg) and immersed it in PBS to await the assay. The ATP assay Kit (S0026, Beyotime, China) was employed to quantify ATP levels in the tissue lysates through a colorimetric assay according to the manufacturer's guidelines. Luminescences were tested by the luminometer system (Promega, USA).

Western blot analysis

Cells were lysed using RIPA buffer (Beyotime, China) supplemented with PMSF (Beyotime, China) and quantified using the BCA protein assay kit (Beyotime, China). Equal amounts of protein were separated on SDS-PAGE gels and then transferred to PVDF membranes (Millipore, USA). Incubated with antibodies against ATP1A1 (Proteintech, China), ATP5F1B (Proteintech, China), ATP5J2 (Proteintech, China), P-AMPK (Proteintech, China), and GAPDH (Proteintech, China). Target protein expression levels were detected using the Immobilob™ Western chemiluminescence assay with HRP substrate (Millipore, USA).

Pharmacokinetic Analysis

Blood samples were collected at 0.083, 0.25, 0.5, 1, 2, 3, 4, 6, 8, 18, and 24 hours following a single oral dose of 5 mg/kg IACS-010759 in mice. Plasma was extracted and analyzed by LC-MS/MS for IACS-010759 concentration. Non-compartmental analysis was performed using the DAS2.0 pharmacokinetic program to estimate pharmacokinetic parameters, including maximum plasma concentration (Cmax), time to reach maximum concentration (tmax), half-life (t1/2), area under the concentration-time curve (AUC), minimum required level (MRL), and oral clearance (CL).

Conclusions

This study offers a cutting-edge perspective on the issue of age differences among breast cancer patients. We identify a defining high metabolic, ATP synthesis-enriched subpopulation that is strongly associated with young BC aggressiveness, present even in adjacent normal tissue, suggesting an age

dependent metabolic predisposition. Critically, we provide preclinical proof of concept that targeting this metabolic hyperactivity represents a promising, age specific therapeutic avenue for young BC patients, who currently face disproportionately worse outcomes. Our findings highlight the necessity of age tailored diagnostic and therapeutic strategies in BC management. Future efforts should focus on validating these metabolic and immune signatures as biomarkers and translating metabolic targeting into clinical trials for young women with this aggressive disease.

Declarations

Ethics approval and consent to participate

This study involving animal participants was reviewed and approved by Ethics Committee of the Affiliated Huaian No.1 People's Hospital of Nanjing Medical University (DW-P-2024-034-01).

Consent for publication

All the authors have approved the manuscript.

Competing interests

The authors declare no competing interests.

Author Contributions

JiangYang Wan, RuiPeng Zhao and Chen Zhang designed the study. JiangYang Wan, Rui Peng Zhao, Chen Zhang, Wei Song, LinLin Zhen and DongZhu Da carried out the study. JiangYang Wan drafted the manuscript. JiangYang Wan, RuiPeng Zhao and Chen Zhang analyzed the data and made the graphics. All authors contributed to the article and approved the submitted version. Zhi Li is the guarantor of the study.

Funding

This work was supported by the National Natural Science Foundation of China (82403191), Jiangsu Provincial Double-Innovation Doctor Program (JSSCBS20222034), the Natural Science Research Program of Huai'an, Jiangsu, China (HAB202301), Science and Technology Development Funding of Nanjing Medical University (NMUB20230103) and the Affiliated Huai'an Clinical Hospital Foundation of Xuzhou Medical University (XYFY202310).

Acknowledgements

We are grateful to all the funds that have supported our research.

Availability of Data and Materials

The datasets used and analyzed during the current study are available from the corresponding author on reasonable request.

References

1. Sung H, Ferlay J, Siegel RL, Laversanne M, Soerjomataram I, Jemal A, et al. Global Cancer Statistics 2020: GLOBOCAN Estimates of Incidence and Mortality Worldwide for 36 Cancers in 185 Countries. CA Cancer J Clin. 2021;71(3):209–49.
2. Eklund M, Esserman LJ. Screening: biology dictates the fate of young women with breast cancer. Nat Rev Clin Oncol. 2013;10(12):673–5.
3. Azim HA, Michiels S, Bedard PL, Singhal SK, Criscitiello C, Ignatiadis M, et al. Elucidating prognosis and biology of breast cancer arising in young women using gene expression profiling. Clin Cancer Res. 2012;18(5):1341–51.
4. Cancello G, Maisonneuve P, Rotmensz N, Viale G, Mastropasqua MG, Pruneri G, et al. Prognosis and adjuvant treatment effects in selected breast cancer subtypes of very young women (< 35 years) with operable breast cancer. Ann Oncol. 2010;21(10):1974–81.
5. Anders CK, Hsu DS, Broadwater G, Acharya CR, Foekens JA, Zhang Y, et al. Young age at diagnosis correlates with worse prognosis and defines a subset of breast cancers with shared patterns of gene expression. J Clin Oncol. 2008;26(20):3324–30.
6. Azim HA, Partridge AH. Biology of breast cancer in young women. Breast Cancer Res. 2014;16(4):427.
7. Ingebriktsen LM, Svanøe AA, Myrmel Sæle AK, Humlevik ROC, Toska K, Kalvenes MB, et al. Age-Related Clusters and Favorable Immune Phenotypes in Young Breast Cancer Patients. Mod Pathol. 2024;37(8):100529.
8. Mahdavi R, Yousefpour N, Abbasvandi F, Ataee H, Hoseinpour P, Akbari ME, et al. Intraoperative pathologically-calibrated diagnosis of lymph nodes involved by breast cancer cells based on electrical impedance spectroscopy; a prospective diagnostic human model study. Int J Surg. 2021;96:106166.
9. Lafzi A, Moutinho C, Picelli S, Heyn H. Tutorial: guidelines for the experimental design of single-cell RNA sequencing studies. Nat Protoc. 2018;13(12):2742–57.
10. Ståhl PL, Salmén F, Vickovic S, Lundmark A, Navarro JF, Magnusson J, et al. Visualization and analysis of gene expression in tissue sections by spatial transcriptomics. Science. 2016;353(6294):78–82.
11. Viale A, Pettazzoni P, Lyssiotis CA, Ying H, Sánchez N, Marchesini M, et al. Oncogene ablation-resistant pancreatic cancer cells depend on mitochondrial function. Nature. 2014;514(7524):628–32.
12. Hanahan D. Hallmarks of Cancer: New Dimensions. Cancer Discov. 2022;12(1):31–46.
13. DeBerardinis RJ, Chandel NS. Fundamentals of cancer metabolism. Sci Adv. 2016;2(5):e1600200.

14. LeBleu VS, O'Connell JT, Gonzalez Herrera KN, Wikman H, Pantel K, Haigis MC et al. PGC-1α mediates mitochondrial biogenesis and oxidative phosphorylation in cancer cells to promote metastasis. Nat Cell Biol. 2014;16(10).
15. Pavlova NN, Thompson CB. The Emerging Hallmarks of Cancer Metabolism. Cell Metab. 2016;23(1):27–47.
16. Lee ACK, Lau PM, Kwan YW, Kong SK. Mitochondrial Fuel Dependence on Glutamine Drives Chemo-Resistance in the Cancer Stem Cells of Hepatocellular Carcinoma. Int J Mol Sci. 2021;22(7).
17. Sabharwal SS, Schumacker PT. Mitochondrial ROS in cancer: initiators, amplifiers or an Achilles' heel? Nat Rev Cancer. 2014;14(11):709–21.
18. Sas K, Szabó E, Vécsei L, Mitochondria. Oxidative Stress and the Kynurenine System, with a Focus on Ageing and Neuroprotection. Molecules. 2018;23(1).
19. Faubert B, Solmonson A, DeBerardinis RJ. Metabolic reprogramming and cancer progression. Science. 2020;368(6487).
20. Uslu C, Kapan E, Lyakhovich A. OXPHOS inhibition overcomes chemoresistance in triple negative breast cancer. Redox Biol. 2025;83:103637.
21. Vijayan D, Young A, Teng MWL, Smyth MJ. Targeting immunosuppressive adenosine in cancer. Nat Rev Cancer. 2017;17(12):709–24.
22. Shapiro RM, Birch GC, Hu G, Vergara Cadavid J, Nikiforow S, Baginska J et al. Expansion, persistence, and efficacy of donor memory-like NK cells infused for posttransplant relapse. J Clin Invest. 2022;132(11).
23. Guo C, Li B, Ma H, Wang X, Cai P, Yu Q, et al. Single-cell analysis of two severe COVID-19 patients reveals a monocyte-associated and tocilizumab-responding cytokine storm. Nat Commun. 2020;11(1):3924.
24. Qiu X, Mao Q, Tang Y, Wang L, Chawla R, Pliner HA, et al. Reversed graph embedding resolves complex single-cell trajectories. Nat Methods. 2017;14(10):979–82.
25. Kilkenny C, Browne WJ, Cuthill IC, Emerson M, Altman DG. Improving bioscience research reporting: the ARRIVE guidelines for reporting animal research. PLoS Biol. 2010;8(6):e1000412.
26. Hanahan D, Weinberg RA. Hallmarks of cancer: the next generation. Cell. 2011;144(5):646–74.
27. López-Otín C, Blasco MA, Partridge L, Serrano M, Kroemer G. The hallmarks of aging. Cell. 2013;153(6):1194–217.
28. Lee G, Auffinger B, Guo D, Hasan T, Deheeger M, Tobias AL, et al. Dedifferentiation of Glioma Cells to Glioma Stem-like Cells By Therapeutic Stress-induced HIF Signaling in the Recurrent GBM Model. Mol Cancer Ther. 2016;15(12):3064–76.
29. Kahles A, Lehmann K-V, Toussaint NC, Hüser M, Stark SG, Sachsenberg T et al. Comprehensive Analysis of Alternative Splicing Across Tumors from 8,705 Patients. Cancer Cell. 2018;34(2).
30. Chang C-H, Qiu J, O'Sullivan D, Buck MD, Noguchi T, Curtis JD, et al. Metabolic Competition in the Tumor Microenvironment Is a Driver of Cancer Progression. Cell. 2015;162(6):1229–41.

31. Galon J, Bruni D. Approaches to treat immune hot, altered and cold tumours with combination immunotherapies. Nat Rev Drug Discov. 2019;18(3):197–218.
32. Fulop T, Larbi A, Dupuis G, Le Page A, Frost EH, Cohen AA, et al. Immunosenescence and Inflamm-Aging As Two Sides of the Same Coin: Friends or Foes? Front Immunol. 2017;8:1960.
33. McWilliam HEG, Villadangos JA. MR1 antigen presentation to MAIT cells and other MR1-restricted T cells. Nat Rev Immunol. 2024;24(3):178–92.
34. Gambardella V, Alfaro-Cervelló C, Cejalvo JM, Tapia M, Cervantes A. the literature: August 2021. ESMO Open. 2021;6(5):100247.
35. Rossi EL, de Angel RE, Bowers LW, Khatib SA, Smith LA, Van Buren E, et al. Obesity-Associated Alterations in Inflammation, Epigenetics, and Mammary Tumor Growth Persist in Formerly Obese Mice. Cancer Prev Res (Phila). 2016;9(5):339–48.
36. Molina JR, Sun Y, Protopopova M, Gera S, Bandi M, Bristow C, et al. An inhibitor of oxidative phosphorylation exploits cancer vulnerability. Nat Med. 2018;24(7):1036–46.
37. Evans KW, Yuca E, Scott SS, Zhao M, Paez Arango N, Cruz Pico CX, et al. Oxidative Phosphorylation Is a Metabolic Vulnerability in Chemotherapy-Resistant Triple-Negative Breast Cancer. Cancer Res. 2021;81(21):5572–81.
38. Altea-Manzano P, Doglioni G, Liu Y, Cuadros AM, Nolan E, Fernández-García J, et al. A palmitate-rich metastatic niche enables metastasis growth via p65 acetylation resulting in pro-metastatic NF-κB signaling. Nat Cancer. 2023;4(3):344–64.

Figures

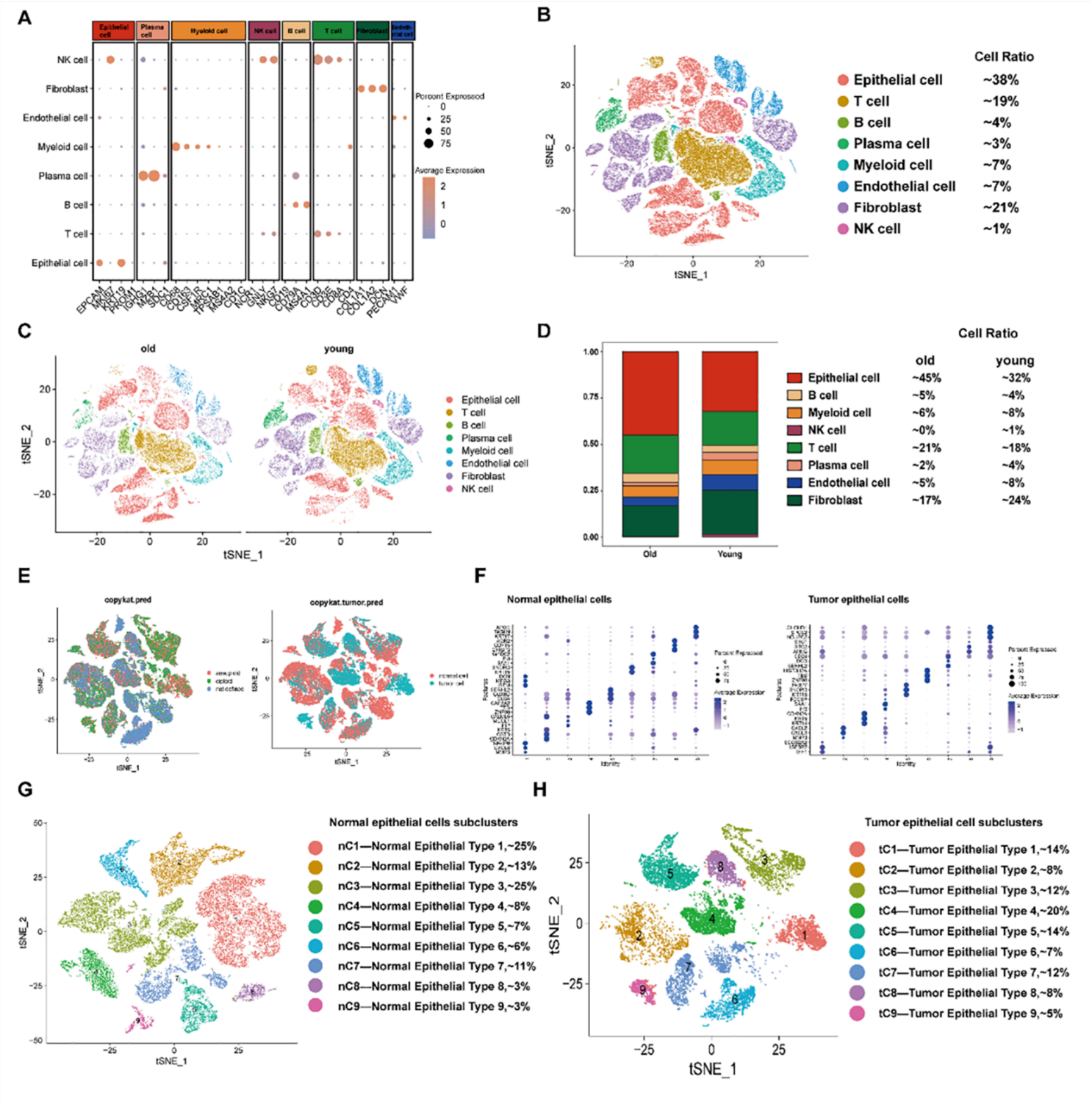


Figure 1

Comprehensive scRNA-seq analysis unveils the cellular landscape of breast tumors in the young and aged groups. (A) Dot plot showing the expression of characteristic genes of different cell types. (B) tSNE visualization of cell composition in breast tumors. (C) tSNE visualization of different cell composition in the young and aged breast tumors. (D) Bar plot indicating the cell composition proportions in the young and aged groups. (E) tSNE projection of tumor and normal epithelial cells predicted by Copycat. (F) Dot plot showing the expression of characteristic genes of 9 epithelial subclusters in the young and aged

groups. (G) tSNE visualization of subclusters' composition in the young group. (H) tSNE visualization of subclusters' composition in the aged group.

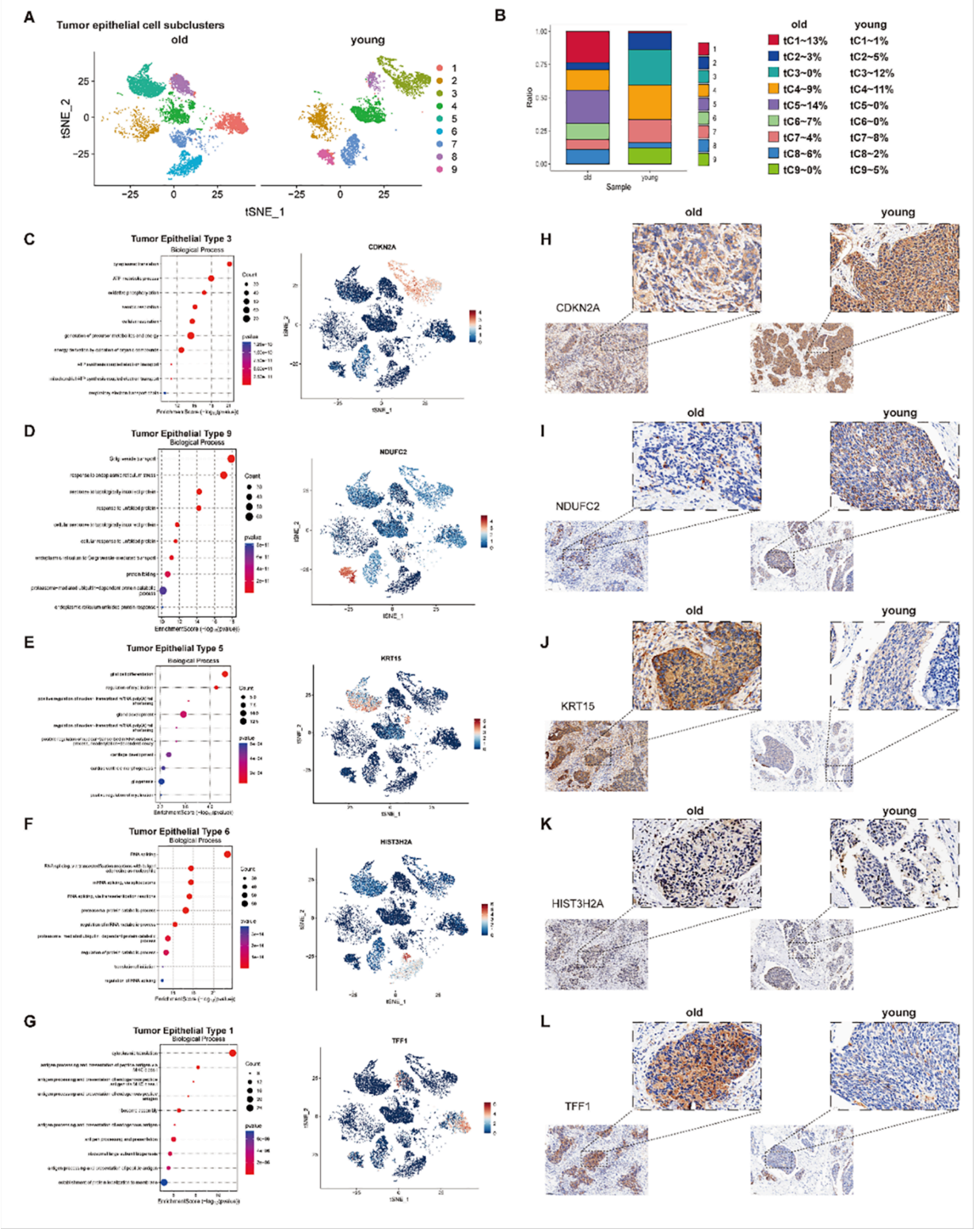


Figure 2

Tumor epithelial cells reveal distinct cell populations between the young and the aged. (A) tSNE visualization of 9 tumor epithelial cell subclusters composition in the young and aged groups. (B) Bar

plot indicating 9 tumor epithelial cell subclusters in the young and aged groups. (C) GO enrichment analysis of marker genes in tumor epithelial Type 3. tSNE projection of CDKN2A in tumor epithelial cells. (D) GO enrichment analysis of marker genes in tumor epithelial Type 9. tSNE projection of NDUFC2 in tumor epithelial cells. (E) GO enrichment analysis of marker genes in tumor epithelial Type 5. tSNE projection of KRT15 in tumor epithelial cells. (F) GO enrichment analysis of marker genes in tumor epithelial Type 6. tSNE projection of HIST32A in tumor epithelial cells. (G) GO enrichment analysis of marker genes in tumor epithelial Type 1. tSNE projection of TFF1 in tumor epithelial cells. (H) IHC:expression of CDKN2A in breast cancer tissues in the young and aged (I) IHC:expression of NDUFC2 in breast cancer tissues in the young and aged. (J) IHC:expression of KRT15 in breast cancer tissues in the young and aged. (K) IHC:expression of HIST32A in breast cancer tissues in the young and aged. (K) IHC:expression of TFF1 in breast cancer tissues in the young and aged.

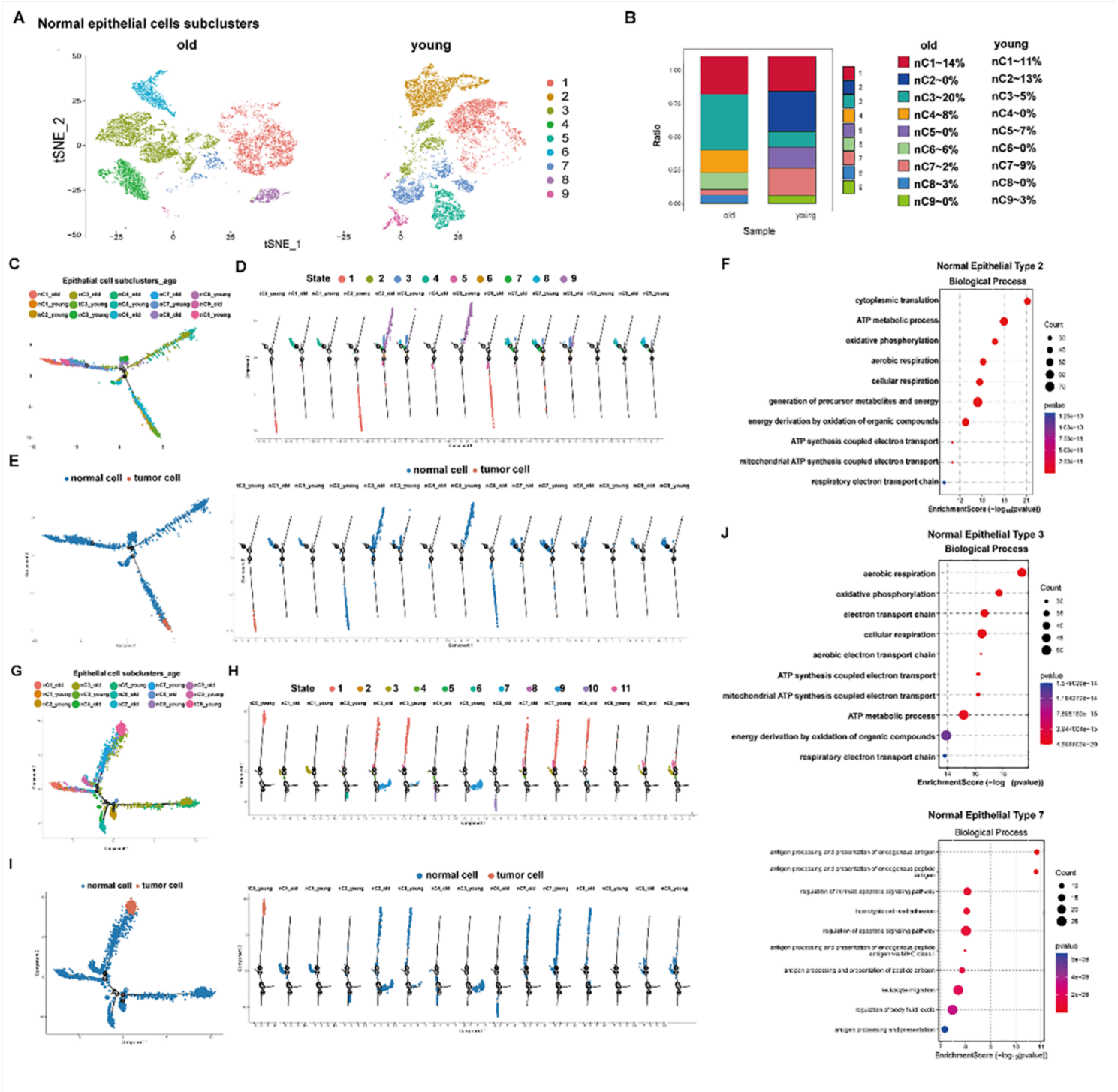


Figure 3

Normal epithelial cell subclusters reveal distinct trajectories in the young group. (A) tSNE visualization of 9 normal epithelial cell subclusters composition in the young and aged groups. (B) Bar plot indicating 9 normal epithelial cell subclusters in the young and aged groups. (C) Cell trajectory analysis for the 9 normal epithelial subclusters and tumor epithelial type 3 subcluster. (D) Pseudotime trajectory colored according to cell state. (E) Pseudotime trajectory colored according to cell type. (F) GO enrichment analysis of marker genes in normal epithelial Type 2. (G) Cell trajectory analysis for the 9 normal epithelial subclusters and tumor epithelial type 9 subcluster. (H) Pseudotime trajectory colored

according to cell state. (I) Pseudotime trajectory colored according to cell type. (J) GO enrichment analysis of marker genes in normal epithelial Type 3 and Type 7.

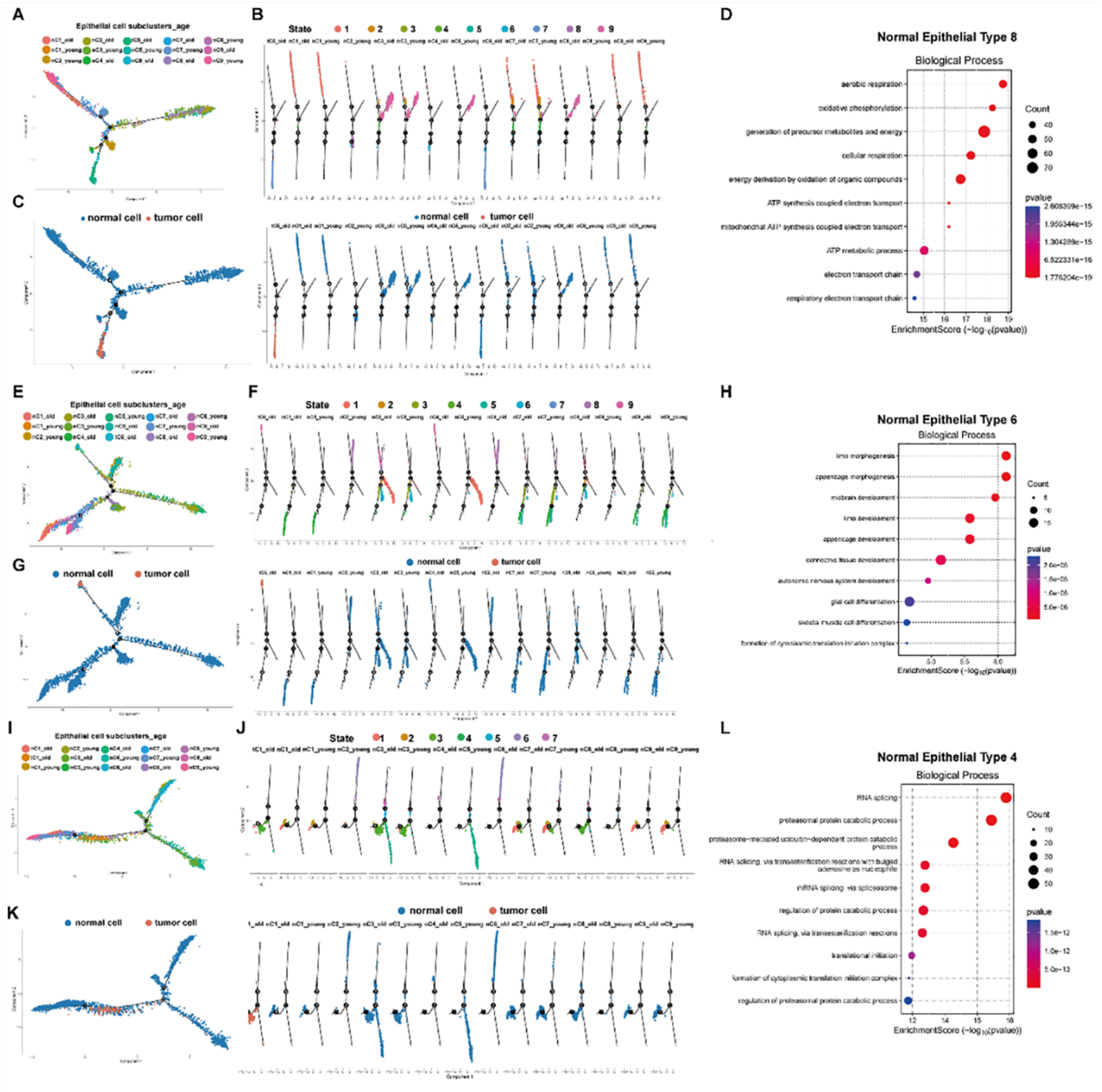


Figure 4

Normal epithelial cell subclusters reveal distinct trajectories in the aged group. (A) Cell trajectory analysis for the 9 normal epithelial subclusters and tumor epithelial type 5 subcluster. (B) Pseudotime trajectory colored according to cell state. (C) Pseudotime trajectory colored according to cell type. (D) GO enrichment analysis of marker genes in normal epithelial Type 2. (E) Cell trajectory analysis for the 9

normal epithelial subclusters and tumor epithelial type 6 subcluster. (F) Pseudotime trajectory colored according to cell state. (G) Pseudotime trajectory colored according to cell type. (H) GO enrichment analysis of marker genes in normal epithelial Type 6. (I) Cell trajectory analysis for the 9 normal epithelial subclusters and tumor epithelial type 1 subcluster. (J) Pseudotime trajectory colored according to cell type. (K) Pseudotime trajectory colored according to cell type. (L) GO enrichment analysis of marker genes in normal epithelial Type 4.

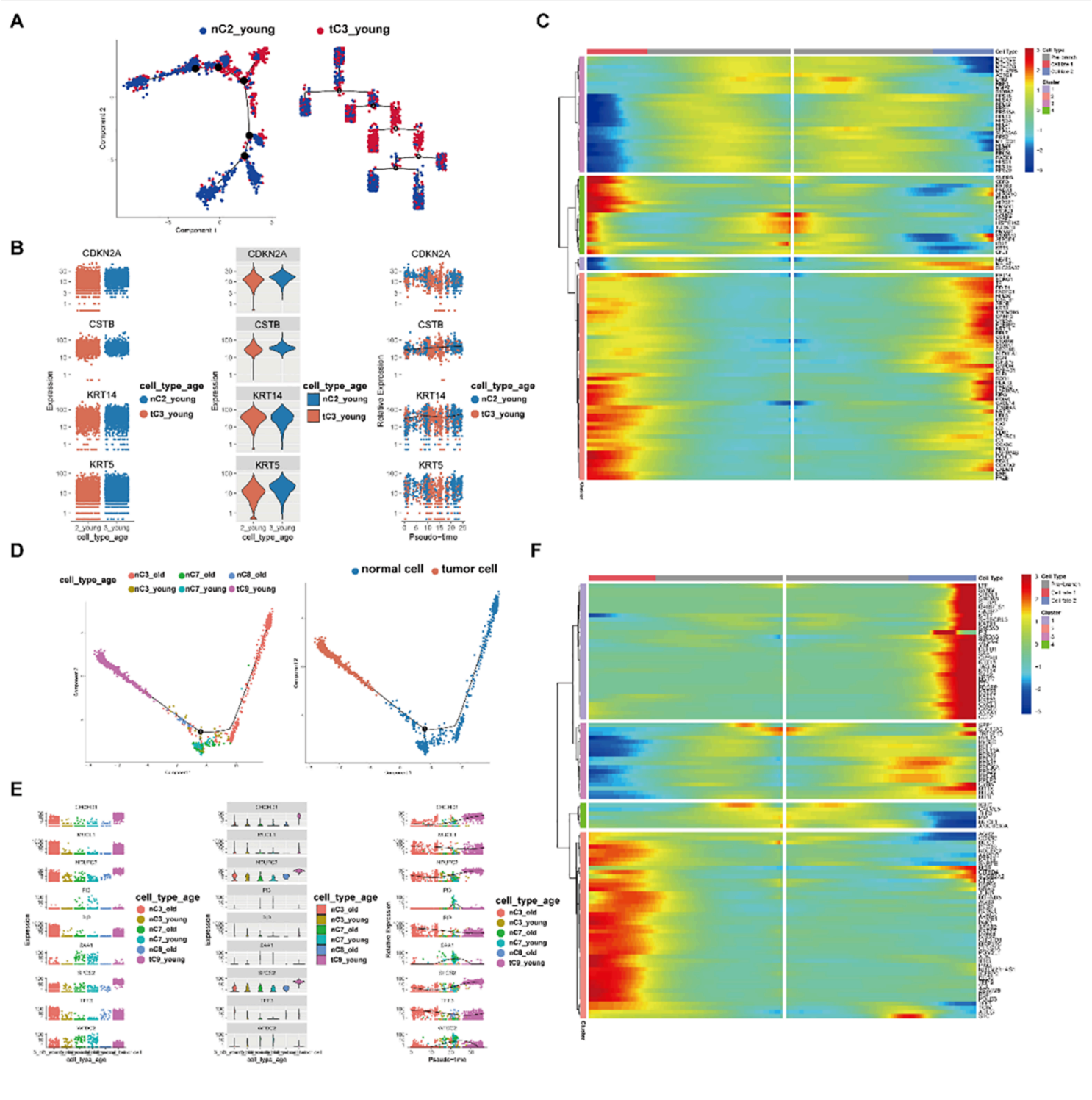


Figure 5

Pseudotime analysis reveals the cell development trajectories of tumor epithelial cells in the young group. (A) Cell trajectory analysis for normal epithelial type 2 subcluster and tumor epithelial type 3 subcluster in the young group. (B) The expression of top marker genes of tumor epithelial type 3 subcluster in the cell trajectory. (C) Heatmap showing expression profiles of different cell fates along pseudotime. DEGs (qval<1e-5) are hierarchically clustered into four subclusters. (D)Cell trajectory analysis for normal epithelial type 3,7,8 subclusters and tumor epithelial type 9 subcluster in the young group. (E) The expression of top marker genes of tumor epithelial type 9 subcluster in the cell trajectory. (F) Heatmap showing expression profiles of different cell fates along pseudotime. DEGs (qval<1e-5) are hierarchically clustered into four subclusters.

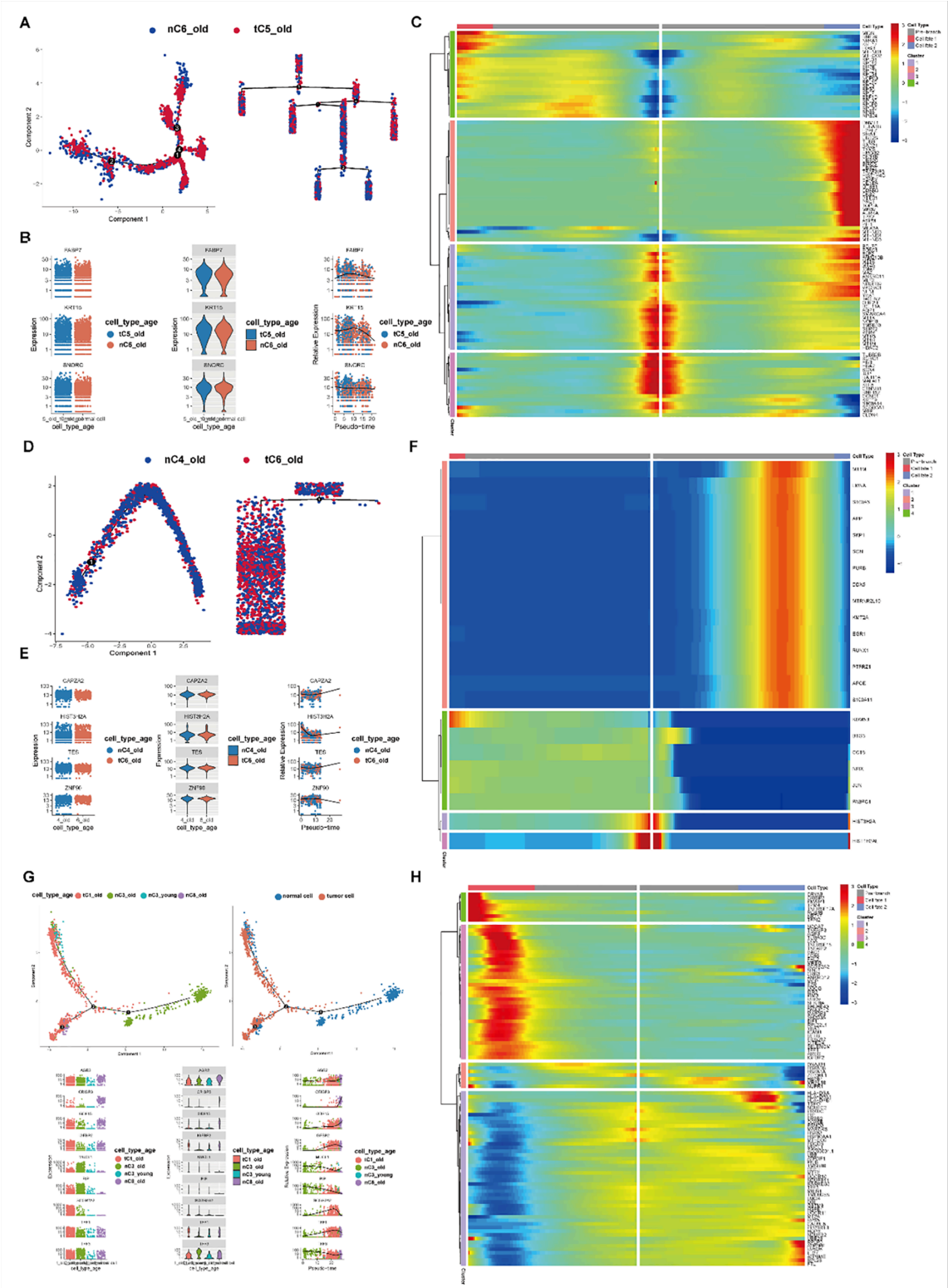


Figure 6

Pseudotime analysis reveals the cell development trajectories of tumor epithelial cells in the aged. (A) Cell trajectory analysis for normal epithelial type 2 subcluster and tumor epithelial type 3 subcluster in the young group. (B) The expression of top marker genes of tumor epithelial type 3 subcluster in the cell trajectory. (C) Heatmap showing expression profiles of different cell fates along pseudotime. DEGs (qval<1e-5) are hierarchically clustered into four subclusters. (D)Cell trajectory analysis for normal

epithelial type 3,7,8 subclusters and tumor epithelial type 9 subcluster in the young group. (E) The expression of top marker genes of tumor epithelial type 9 subcluster in the cell trajectory. (F) Heatmap showing expression profiles of different cell fates along pseudotime. DEGs (qval<1e-5) are hierarchically clustered into four subclusters. (A) Cell trajectory analysis for normal epithelial type 2 subcluster and tumor epithelial type 3 subcluster in the young group. (B) The expression of top marker genes of tumor epithelial type 3 subcluster in the cell trajectory. (C) Heatmap showing expression profiles of different cell fates along pseudotime. DEGs (qval<1e-5) are hierarchically clustered into four subclusters.

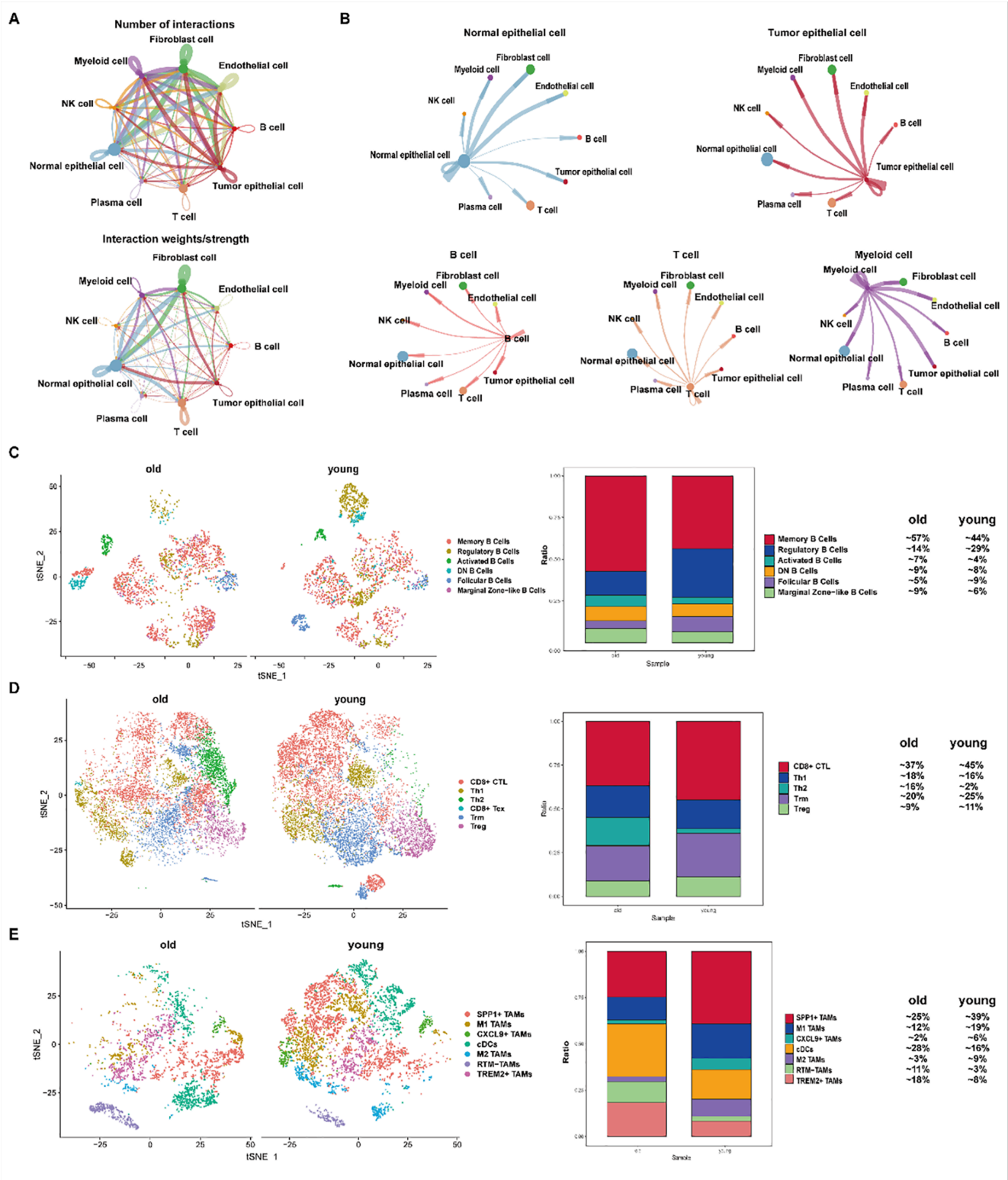


Figure 7

Cell-cell communication in the young group and distinct immune cell populations between the young and aged. (A) The cell–cell communication network among different cell types in the young group. (B) Comparative analysis of intercellular communication networks in the young group included: (I) normal epithelial cells versus other cell types; (II) tumor epithelial cells versus other cell types; and (III) major immune cell types versus other cell types. (C) tSNE visualization of B cells composition in the young and aged groups. Bar plot indicating B cell subclusters in the young and aged groups. (D) tSNE visualization of T cells composition in the young and aged groups. Bar plot indicating T cell subclusters in the young and aged groups. (E) tSNE visualization of Myeloid cells composition in the young and aged groups. Bar plot indicating Myeloid cell subclusters in the young and aged groups.

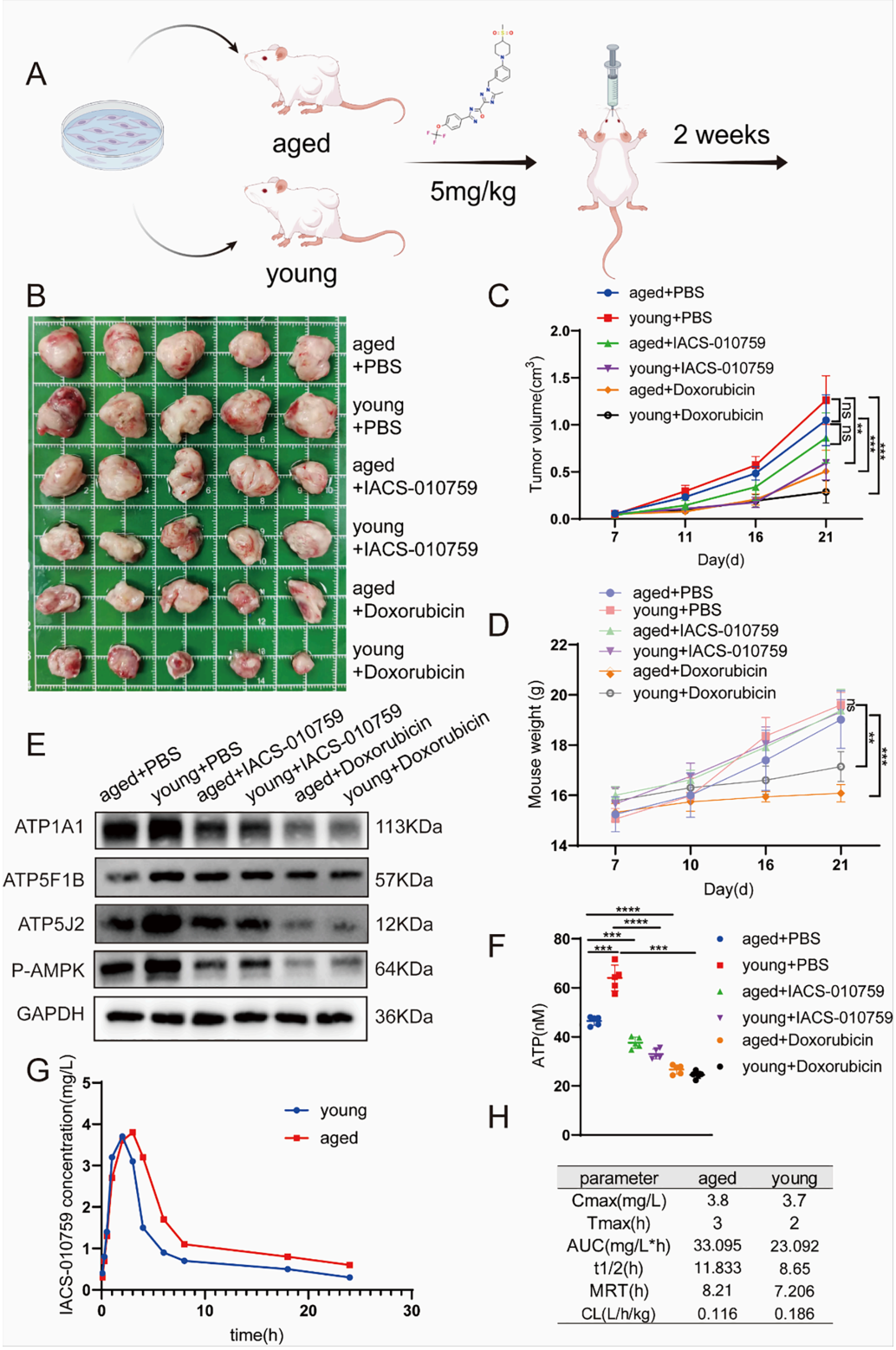


Figure 8

IACS-010759 effectively inhibited young breast cancer progression in mice. (A) Diagram of animal modeling and treatment. (B) Tumor removed and photographed. (C) Recorded tumor volume and generate growth curves. (D) Recording of body weight gain in mice. (E) Expression levels of oxidative phosphorylation-related proteins in tumor tissues from each group of mice. (F) ATP contents were detected in different groups of tumor tissues. (G) Plasma pharmacokinetic profiles following a single

oral dose of IACS-010759 in young and aged mice. (H) Non-compartmental analysis was performed to estimate pharmacokinetic parameters in young and aged mice.

Supplementary Files

This is a list of supplementary files associated with this preprint. Click to download.

- SupplementaryInformation.docx
- TableS1.pdf
- TableS2.pdf
- SupplementaryWB.pdf